Acousto-optical nanoscopy of buried photonic nanostructures

T. Czerniuk[1,*], C. Schneider[2], M. Kamp[2], S. Höfling[2], B. A. Glavin[3], D. R. Yakovlev[1,4], A. V. Akimov[5], and M. Bayer[1,4]

[1]Experimentelle Physik 2, Technische Universität Dortmund, 44221 Dortmund, Germany
[2]Technische Physik, Universität Würzburg, 97074 Würzburg, Germany
[3]V. E. Lashkaryov Institute of Semiconductor Physics, 03028 Kyiv, Ukraine
[4]Ioffe Institute, Russian Academy of Sciences, 194021 St. Petersburg, Russia
[5]School of Physics and Astronomy, University of Nottingham, Nottingham NG7 2RD, United Kingdom
[*]Corresponding author: Thomas.Czerniuk@tu-dortmund.de

Compiled April 12, 2017

We develop a nanoscopy method with in-depth resolution for layered photonic devices. Photonics often require tailored light field distributions for the operated optical modes and an exact knowledge of the geometry of a device is crucial to assess its performance. We present an acousto-optical nanoscopy method for the characterization of layered photonic structures based on the uniqueness of the light field distributions: for a given wavelength, we record the reflectivity modulation during the transit of a picosecond acoustic pulse. The obtained temporal profile can be linked to the internal light field distribution. From this information, a reverse-engineering procedure allows us to reconstruct the light field and the underlying photonic structure very precisely. We apply this method to the slow light mode of an AlAs/GaAs micropillar resonator and show its validity for the tailored experimental conditions.

OCIS codes: (140.3490) Lasers, distributed feedback; (060.2420) Fibers, polarization-maintaining;(060.3735) Fiber Bragg gratings.

http://dx.doi.org/10.1364/optica.XX.XXXXXX

1. INTRODUCTION

Photonic nanostructures, in which light can be guided or confined, are fundamental for a wide range of applications ranging from information communication to cavity-quantum-electrodynamics and optomechanics. The geometry and the constituting materials of the structure define the optical resonances and the spatial profile of the associated photonic modes. In the case of optical cavities for example, photons are slowed down or trapped in localized modes to obtain lifetimes of up to milliseconds [1]. The light-matter-interaction with an optically active material is drastically enhanced, provided that it is placed at a maximum of the light field distribution of such a long-lived mode. There are manifold challenging applications in the strong coupling regime like bright single photon sources [2], entangled photons [3] or polariton lasing [4], for which the exact knowledge of the resonator's geometry and photonic field inside the nanostructure are crucial. Information about the surface of the fabricated structures is usually obtained with high resolution by scanning electron microscopy (SEM) or atomic force microscopy (AFM). When in-depth information is desired, transmission electron microscopy (TEM), X-ray diffraction are used. The first one is destructive due to the required cross-sectional cuts. Often these techniques are not easy to access and to handle. In this case an established technique is to record the optical reflectivity spectrum and fit simulations based on a transfer matrix approach to the experimental data [5]. The drawback of this method in complicated multilayer structures is that it offers ambiguous in-depth information, since the reflectivity spectrum is an integrated measure determined by the whole structure.

For the nanoscopy of buried films and interfaces picosecond ultrasonics provides a suitable tool [6–9]. A picosecond acoustic

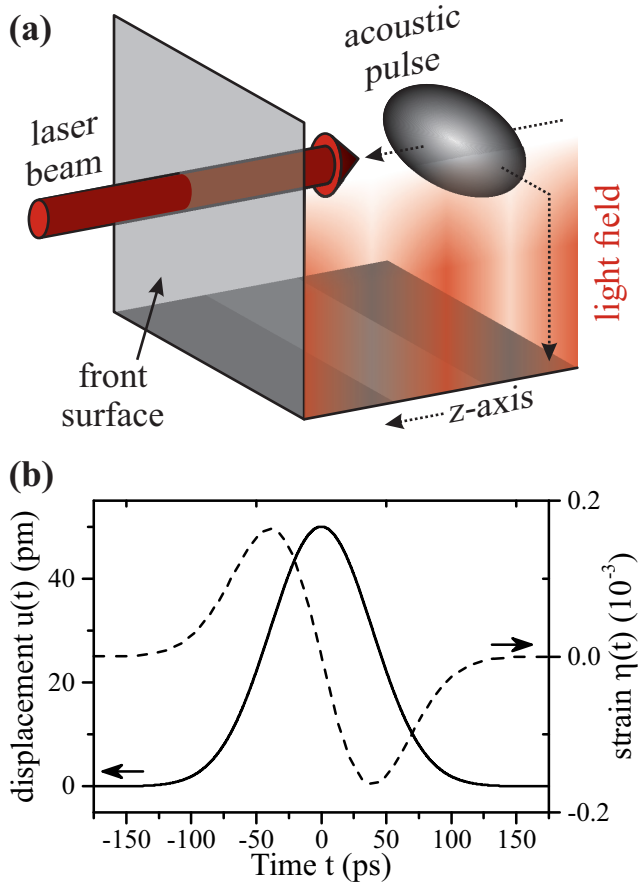

Fig. 1. Sketch of the technique. Panel (a): A laser beam builds up a unique light field distribution (red) inside the structure, while an acoustic pulse simultaneously propagates along the z-axis. The acoustic pulse locally changes the optical properties of the photonic device, which is observable in the reflected intensity of the laser beam. Panel (b): sketch of an acoustic pulse, showing the acoustic displacement (solid line) and the mechanical strain (dashed line).

pulse is optically generated and detected in a photonic nanostructure and allows one to derive information about the position of the internal interfaces. The success of this technique is due to the short wavelengths (down to 10 nm) of the coherent phonons forming the acoustic pulse, which made it possible to investigate buried optical microcavities [10], superlattices [11, 12], hetero-interfaces [13], quantum wells [14], and defects in contacts [15]. Most of the picosecond acoustic experiments in photonic devices were aimed to study specific phononic features arising from the acoustic mismatch between the constituting materials, while their optical properties were considered mainly for the purpose of understanding the generation or detection of THz and sub-THz phonons [7, 16, 17].

The efficiency of picosecond ultrasonics relies on a mismatch of the acoustic properties of the constituting materials, which is not necessarily given. On the contrary, the proposed method of this work is based on obtaining information about the unique light field distribution in the device under study. It only requires contrasting dielectric functions, which is an intrinsic feature of most photonic devices. The difficulty arises from the complex interplay of a picosecond acoustic pulse with the light field in a photonic device. This interplay has been comprehensively described in a number of publications [18, 19]. It turns out, that the properties of (i) the acoustic pulse, namely its duration, the phonon spectrum, and the phonon dispersion in the photonic device, the (ii) light field distribution and (iii) the different mechanisms of light-matter-interaction, like phonon-photon and phonon-electron scattering need to be considered for a complete understanding. Previous works were so far not aimed at deducing unambiguous information about the light field from the overall response [17, 20]. The route to achieve this is to know all other parameters exactly such that they can be eliminated from the response. How this condition can be fulfilled for a practical photonic device by a proper design of the acoustic pulse and choice of the studied light field, is discussed in the present paper.

The basic experimental scheme of the method is presented in Fig. 1 (a): a laser beam is directed onto the nanostructure and builds up the light field sketched in red. The investigated device imprints a unique field distribution, which is exploited for its characterization. A picosecond acoustic pulse is injected into the structure from its backside and propagates with the sound velocity along the z-axis towards the surface of the nanostructure. The temporal displacement profile $u(t)$ can often be modeled by a Gaussian [21] with a duration that depends on the experimental conditions (excitation energy, temperature, nonlinear phenomena) and ranges from several picoseconds up to $\sim$100 ps [21]. In our model we shall use an amplitude of several ten picometer and a full width at half maximum (FWHM) of about 90 ps, like shown in Fig. 1 (b) by the solid line. The derivative of the displacement is associated with the strain $\eta(t)$ and shown in Fig. 1 (b) by the dashed line. The presence of the acoustic pulse slightly perturbs the light field in the structure. For the incident laser beam, this local perturbation leads to a change of the total reflectivity that depends on the light field intensity at the position z of the acoustic pulse. The result for the simplest case of an optically homogeneous material is well known and described by the so-called coherent Brillouin-oscillations originating from the interference of two optical beams: one being reflected from the surface and the other one in the depth of the material, where the acoustic pulse dynamically modifies the optical properties due to the photoelastic effect [22]. For periodic multilayered structures, like distributed Bragg reflectors (DBRs), the oscillation spectrum is more complicated [16, 23] and defined by the photon-phonon momentum conservation also including folded Brillouin-oscillations, which involve phonon-Umklapp-processes [12, 24].

Our aim is to record the reflectivity modulation for more complex photonic nanostructures, when the analysis cannot be based on the momentum conservation only. In the paper we present at first an analytical equation, which allows us to link the reflectivity modulation to the internal light field distribution along the propagation direction of the acoustic pulse. Afterwards we demonstrate that the obtained information can be used to reconstruct the light field, which then in turn is exploited for the characterization of a model multilayer system. In the experimental part of the paper, we apply this technique to a slow photonic mode in a GaAs/AlAs micropillar resonator that falls into the high energy flank of the first optical stop band. We show that the experimentally measured temporal evolution of the reflectivity allows us to precisely calculate the underlying light field distribution and to determine the geometry of the photonic resonator with in depth-resolution and an accuracy of a few nm.

2. THEORETICAL BACKGROUND

The interaction of a picosecond acoustics perturbation with the light field in a photonic nanostructure is due to two fundamentally different contributions, namely (i) the photoelastic effect and (ii) the interface displacement [18]. The photoelastic effect on the one hand is based on the fact that the strain $\eta(z,t)$ leads to a local change of the refractive index Δn. In semiconductors, for photon energies not far from the band gap E_G, Δn can be approximated by

$$\Delta n = \frac{\partial n}{\partial E_G}\frac{\partial E_G}{\partial \eta}\eta. \quad \textbf{(1)}$$

It depends on the dispersion of the refractive index and on the deformation potential constant linking the shift of the energy gap E_G to the applied strain [12, 18]. On the other hand, the interface displacement effect is related to the reflections originating from the surface and the internal material interfaces of the photonic nanostructure. The acoustic pulse modifies their interference terms, since it moves such an interface when passing it, thereby leading to a phase shift of the reflection originating from there. For the description of the acoustic pulse we consider a one-dimensional case. Furthermore, we shall assume that the phonon dispersion is not affected by the nanostructure and may be described by a linear relation between the phonon frequency ω and wavevector q_z

$$\omega = v q_z \quad \textbf{(2)}$$

with the slope given by the longitudinal sound velocity v. In one dimensional periodic nanostructures with a total length much longer than the phonon wavelength, both contributions to the light-matter-interaction result in an optical reflectivity modulation whose spectrum is governed by the photon-phonon momentum conservation including Umklapp-processes

$$q = 2\left|k \pm mG\right|. \quad \textbf{(3)}$$

Here, k is the photon wavevector, G the reciprocal-lattice vector, and m an integer. In most periodic photonic nanostructures for light in the visible to near infrared range, this corresponds to phonon frequencies from zero to several tens of GHz, depending on k [12].

For non-periodic multilayer structures, Eq. (3) is not valid and transfer matrix calculations may be considered for numerical simulations. Our aim is to find experimental conditions under which the treatment of the light-matter-interaction is as simple as possible, e.g. by making one of the two interaction mechanisms negligible. The photoelastic contribution can be turned off by choosing a wavelength where the photoelastic constants are small [25]. Another possibility in the case of a bipolar strain profile [cf. Fig. 1 (b)], like typically generated in picosecond ultrasonics, is to tailor the acoustic spectrum such that the spectral amplitude for high-frequency phonons, which give the major contribution to the photoelastic effect, is small enough for considering only interface displacements [22].

As soon as the photoelastic contribution is minimized by pursuing one or both of the proposed routes, the displacement effect becomes the dominant contribution. In this case, the reflectivity change for a fixed wavelength λ may be expressed analytically by

$$\frac{\Delta R(t)}{R_0} = -k_0 \mathrm{Im}\left[\sum_i \delta\epsilon(z_i)\frac{E^2(z_i)}{r}u(z_i,t)\right], \quad \textbf{(4)}$$

where k_0 is the vacuum photon wave vector and r the complex reflection coefficient of the whole structure (a similar expression was derived in Ref. [18]). The sum runs over all interfaces denoted by i, where z_i marks the position of the interface, $\delta\epsilon(z_i)$ the difference of the dielectric constants at the interfaces, $u(z,t)$ the temporal and spatial displacement profile, and $E(z)$ the normalized, dimensionless, and complex electric field distribution of the considered photonic mode. The electric field has the form $E(z) = \exp(ikz) + r\exp(-ikz)$ at the front surface of the structure at $z = 0$, which determines its phase and amplitude [18]. From this starting point, the distribution $E(z)$ in the whole structure is calculated by a transfer-matrix that also yields the reflection coefficient r [5]. For non-absorbing materials, $\delta\epsilon(z_i)$ is real and one can see that the reflectivity modulation is given by the convolution of the displacement profile with a quantity closely related to the photonic field $\rho(z) = \mathrm{Im}\left(E^2(z)/r\right)$. This convolution is evaluated at discrete sampling points, namely the positions of the interfaces, with a weight determined by the optical contrast.

3. MODEL CALCULATIONS

At first we discuss simulations performed for a planar microcavity structure as an intuitive example for the potential of our method. The bottom and top distributed Bragg reflectors (DBRs) consist of 30 periods of alternating AlAs and GaAs layers with nominal thicknesses of 78 nm and 66 nm, designed for a center stop band wavelength of 925 nm at cryogenic temperatures. Between the two DBRs a λ cavity GaAs spacer is sandwiched. To show the sensitivity of the proposed method to the geometry of the photonic device, an additional scaling factor of (1-x) and (1+x) is afterwards applied to the initial nominal layer thicknesses of the bottom and top DBRs, respectively. In Fig. 2 (a) the calculated reflectivity spectra for two microcavities with rather similar layer thicknesses in the bottom and top DBR are shown ($x = \pm 0.03$). For a wavelength of λ=830 nm close to the stop band edge [indicated by the arrow in Fig. 2 (a)], the different layer thicknesses give rise to a significantly different photonic field distribution $|E(z)|^2$, plotted in Fig. 2 (b). Two features can be seen there: one is a fast oscillatory component, determined by the optical wavelength, and another is a slowly varying envelope function. While the period of the fast oscillations is almost the same in the bottom and top DBR, the periods for the slow ones are different: in the thicker DBR, the envelope function varies on a longer length scale and with a higher relative amplitude than in the thinner DBR. Such striking difference cannot easily be recognized in the reflectivity spectrum shown in Fig. 2 (a). One sees that the central stop band looks almost the same, independent of whether the bottom ($x < 0$, blue curve) or the top ($x > 0$, red curve) DBR is the thicker one. Only in the sidebands slight deviations occur, so that it is hard to distinguish the two different structures from their reflectivity spectra alone.

The specific features of the photonic field, which are not recognized in the reflectivity spectrum, become visible when calculating the reflectivity change induced by an acoustic pulse according to Eq. (4). In Fig. 2 (c) the temporal traces for $\Delta R(t)/R_0$ are presented for a Gaussian displacement pulse with a FWHM of 90 ps propagating in the structure with a mean sound velocity of $\overline{v}$=5230 m/s. Here, the time t=0 ns corresponds to the injection of the acoustic pulse into the bottom DBR and the time $t \approx$1.75 ns to the time when the acoustic pulse reaches the top surface of the top DBR. Both curves show an oscillatory behav-

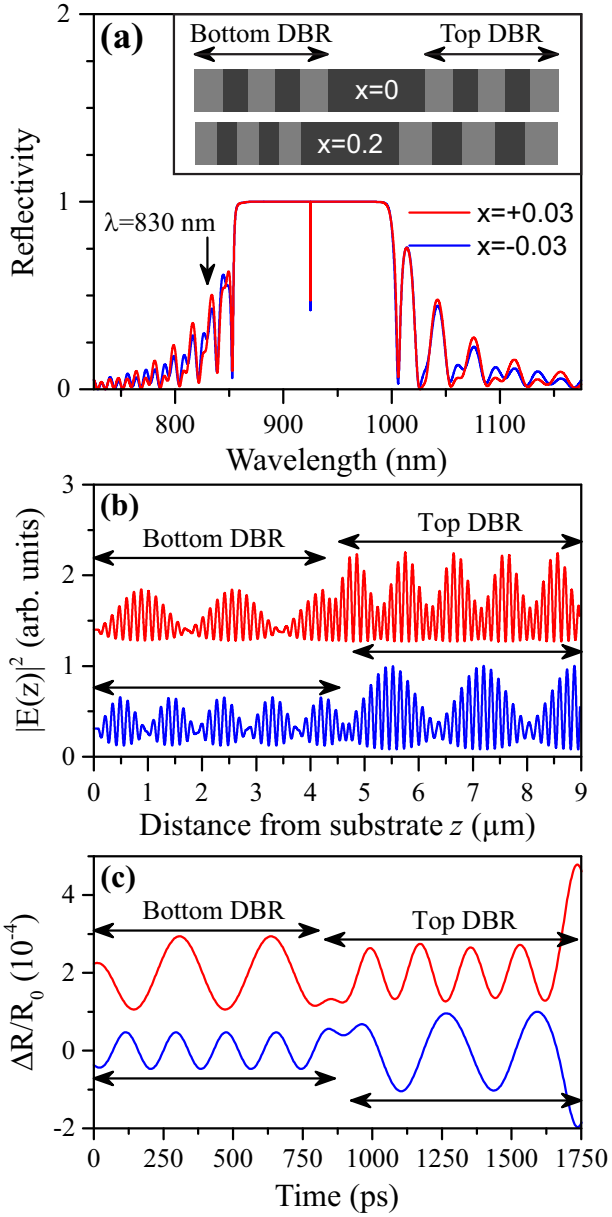

Fig. 2. Simulations for two differently scaled planar microcavities with x=-0.03 (blue curves) and x=+0.03 (red curves). Panel (a): Calculated reflectivity spectra; the arrow marks the wavelength studied in the following. The modeled structure and the influence of x are illustrated in the inset. Panel (b): Light field distributions $|E(z)|^2$ in the two cavities for the wavelength indicated in panel (a). Panel (c): Temporal reflectivity change during the transit of a Gaussian displacement pulse with a FWHM of 90 ps through the device.

ior whose periods resemble the variations of the light field's envelope function: when the acoustic pulse propagates through the DBR with the faster (slower) changing light field envelope, we observe a faster (slower) reflectivity modulation. With these findings one can clearly distinguish between the two differently scaled microcavities.

Note that the oscillations in the reflectivity modulation are not directly proportional to the light field intensity. Although the periods of the oscillations in the thinner and thicker DBRs match very well the period of the corresponding envelope functions, which is also an important information, there is a non-trivial phase difference determined by the complex reflection coefficient r, the width of the displacement pulse, and for absorbing media also the dielectric contrast $\delta\epsilon(z)$. Furthermore, it is necessary to select a probe wavelength λ, whose light field distribution is strongly controlled by the parameters of the photonic device such that small variations of these parameters lead to strong change of the reflectivity modulation. For the microcavity presented here, this means, for example, a probe wavelength close to the optical stop band.

We have shown by transfer matrix calculations that for an acoustic pulse with a width of ∼100 ps, the contribution of the photoelastic effect is negligible and the interface displacement effect according to Eq. (4) governs the temporal evolution of the reflectivity changes (see supplemental content). Due to the relatively long acoustic pulse, the small-period oscillating field does not give any contribution to $\Delta R(t)/R_0$. Moreover, the wavelength λ of the considered light field is chosen to be in the transparency region of AlAs and GaAs (at low temperatures), where the refractive index dispersion is flat and the photoelastic effect is consequently rather inefficient [26]. Although reflections of the acoustic pulse at internal interfaces have been included in the calculations, they do not play an important role here, since the phonon spectrum of the modeled acoustic pulse does not reach frequencies as high as the first phononic stop band at around 18 GHz [10].

4. EXPERIMENT

Experiments to demonstrate the validity of the method in practical photonic devices were performed on micropillar lasers with two DBRs consisting of 33 and 26 periods of alternating AlAs and GaAs layers for the bottom and the top mirror, respectively. The nominal thicknesses of the AlAs and GaAs layers are 74 nm and 69 nm. In between the two DBRs a 266 nm thick λ-cavity GaAs spacer is sandwiched such that the nominal total thickness of the structure is about 8.7 μm. An ensemble of $Al_{0.09}Ga_{0.55}In_{0.36}As$ quantum dots (QDs) is placed in the cavity layer center and serves as the active medium of the laser. Micropillars with different radii ranging from 1.5 μm to 7.5 μm were studied, because they offer a stronger light field confinement than planar structures [27]. We use a time-resolved pump-probe setup to generate the acoustic pulse with the pump and detect the reflectivity modulation with the probe laser beam. Both originate from a pulsed laser with a central wavelength of 800 nm and a spectral width of 10 nm, which falls into the high energy flank of the sample's first optical stop band [cf. Fig. 3 (a)]. The acoustic pulse is generated on the backside of the sample and injected from there into the micropillars [28]. To ensure a lossless transfer through the 220 μm thick GaAs substrate [29], the sample is placed in a flow cryostat and attached to a cold finger kept at a temperature of 8 K. More details about the sample and the experimental setup can be found in the supplement content.

In Fig. 3 (b) the measured reflectivity change $\Delta R(t)/R_0$ obtained for a micropillar with a radius of 7.5 μm is presented as the black curve. At a delay of τ_0 the acoustic pulse reaches the foot of the micropillar. Here we record a peak and a subsequent dip, since the beam spot is approximately larger than the micropillar's diameter and we also collect light which is reflected from the surface next to the micropillar. For increasing delays τ, the acoustic pulse is advancing towards the micropillar top sur-

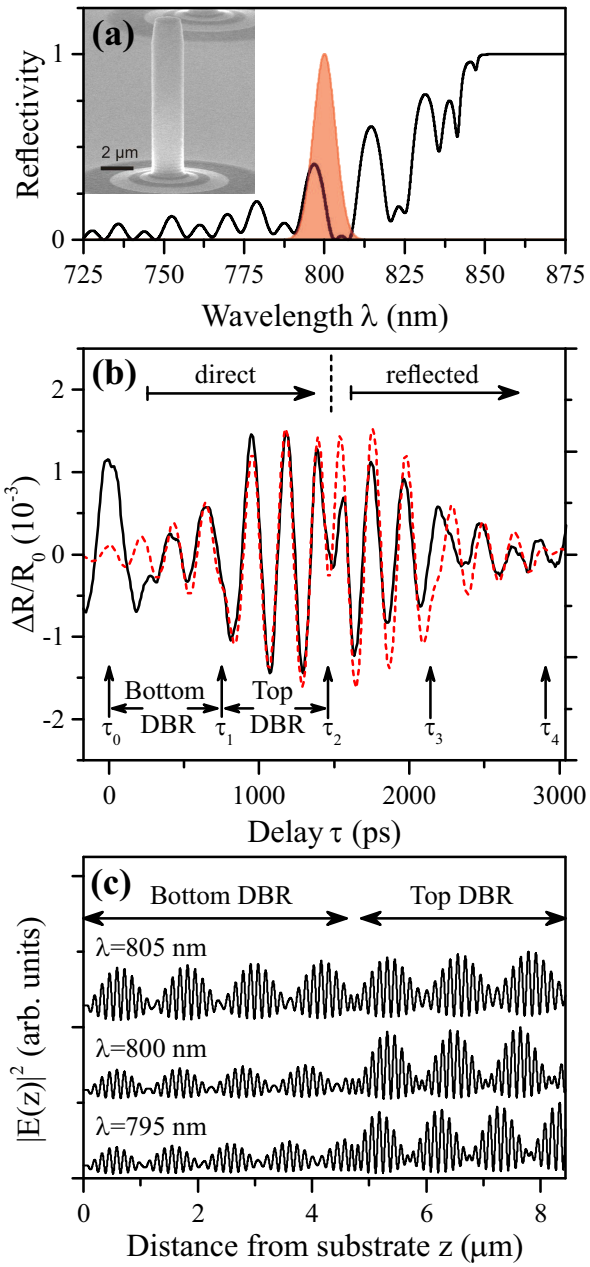

Fig. 3. Experimental measurement of the reflectivity change in an AlAs/GaAs micropillar resonator with a radius of 7.5 μm. Panel (a): Calculated reflectivity spectrum of the micropillar resonator (black) and probe laser spectrum (red area). The inset shows a SEM image of a similar, but thinner, micropillar. Panel (b): Measured reflectivity modulation (black) and simulated curve (red). The arrows mark the specific delays at which the acoustic pulse leaves and enters the DBRs, respectively. Panel (c): Light field distribution $|E|^2$ for the central laser wavelength of 800 nm and for the wavelengths shifted by half the FWHM at 795 nm and 805 nm.

face and is located in the bottom DBR for $\tau_0 < \tau < \tau_1$. Similar to the curves presented in Fig. 2, oscillatory features are recorded there. The temporal separation between the two peaks appearing right before τ_1 is 220±6 ps. After leaving the bottom DBR at τ_1, the acoustic pulse passes through the cavity layer within about 50 ps and enters the top DBR. We observe a phase jump in the signal and afterwards the reflectivity clearly starts to oscillate with a stronger amplitude. The temporal interval between neighboring peaks in the oscillations is 230±6 ps here. These oscillations persist, until the acoustic pulse reaches the top surface of the micropillar at τ_2. Taking the temporal difference between τ_2 and τ_0 of 1.47 ns and the averaged sound velocity in the layered structure of $\overline{v}$=5211 m/s, we conclude that the micropillar has a height of about h=7.7 μm, which corresponds to several doublelayers not etched away in the bottom DBR [cf. Fig. 3 (a)]. At the top of the device, the acoustic pulse is reflected and redirected into the micropillar. In the temporal reflectivity trace this leads to a phase jump at $\tau = \tau_2$. Following the reflection of the acoustic pulse, the reverse sequence is recorded, including the second transit through the cavity layer at τ_3 and so forth. Finally, the acoustic pulse leaves the micropillar at τ_4. The signal at delays $\tau > \tau_4$ is assigned to reflections of the acoustic pulse inside the layered structure and is not considered further.

We compare the measured signal with the simulations according to Eq. (4). The spectral width of the laser pulse of 10 nm needs to be taken into account, which is done by calculating the field distributions for all wavelengths occurring in the laser emission and weighting them by their spectral amplitude [cf. Fig. 3 (a)]. For the acoustic pulse a displacement input profile given by a Gaussian with a FWHM of 90 ps was used. The curve is fitted to the experimental data by scaling the layer thicknesses and the best result is shown as the red dashed curve in Fig. 3 (b). The excellent agreement between the simulated curve and the experiment underlines the validity of our approach. Deviations occur mainly when the acoustic pulse reaches the foot of the micropillar and the reflection from the area next to it is modulated ($\tau = \tau_0$), which is not included in the model. After the reflection of the acoustic pulse from the micropillar surface ($\tau > \tau_2$), we observe in the experiment an asymmetric profile around τ_2, in contrast to the model expectations. This indicates a rough top surface resulting in a diffuse scattering of the phonons in the acoustic wave packet. The field distributions for three wavelengths used in the reversed engineering calculations are displayed in Fig. 3 (c).

Ultimately, the simulation allows us an analysis of our photonic device. We consider three quantities to be extracted from the experimental data: the cavity layer thickness and the mean periodicity in the bottom and top DBR, respectively. Each DBR is assumed to possess its own uniform periodicity, which is obtained for simplicity by rescaling the nominal parameters. The central cavity layer is found to be 2 % (=5.3 nm) thicker than the nominal value of 266 nm by adjusting the relative phase of the oscillations in the top and in the bottom DBR. The period of the oscillations in the bottom and top DBR precisely provide the DBR periodicity. Each GaAs/AlAs DBR layer is found to be about 3.9 % and 4.1 % thinner in the bottom and in the top DBR, respectively. The precision of the found layer thicknesses corresponds to a spatial resolution of a few nanometers for single layers, like in the case of the cavity spacer, where a deviation of 5 nm from the nominal value is found. An even higher resolution is achieved for the *mean* period in periodic structures. Here, the possibility to resolve the different mean layer thicknesses in the bottom and top DBR corresponds to a sub-nanometer resolution. In the experiments, the error for the period of the oscillations is 6 *ps* and determined by the time resolution of the setup, which is governed by the step size of the mechanical delay line rather than by the shorter laser pulse duration. How this error limits the accuracy of the acousto-optical nanoscopy depends strongly on the sensitivity of the probed light field on

structural changes of the device, i.e., the accuracy is a function of the chosen probe wavelength and it is hard to provide an analytical expression for the formal error of the individual layers. Fig. 4 (a) shows the simulated reflectivity change for different cavity layer thicknesses to get an impression of the method's precision. The phase jump at a delay τ_1 indicates the passage of the acoustic pulse from the bottom DBR into the top DBR. While the reflectivity modulation for delays larger than τ_1 is barely affected by the cavity layer thickness, pronounced phase shifts of the oscillations in the bottom DBR are observed. One can see that the chosen curve for a 2 % thinner layer fits much better than the other ones. In the bottom DBR the width of the peaks is too narrow in all simulations. This issue cannot be solved by increasing the duration of the acoustic pulse. Anyway, since the agreement is much better for the top DBR, the width of the peaks is obviously related to the DBR and not to the acoustic pulse. Maybe the quality of the bottom DBR is a bit lower and the thicknesses of the layers are not homogeneous across one oscillation period. Another possible explanation for the broader width of the experimental oscillations might be related to the $Al_{0.09}Ga_{0.55}In_{0.36}As$ quantum dots, whose interaction with the optical field is not included.

We briefly discuss the mechanical eigenmodes supported by the micropillar resonator to exclude that they lead to the observed reflectivity modulation. The pillar's extensional ground mode can be calculated from the height h and the mean sound velocity $\overline{v}$ and is found to have a frequency of 0.15 GHz [30]. The frequency of the radial modes scales inversely with the radius [31]. Such a dependency of the modulation frequency on the radius was not found, when studying a second micropillar with a smaller radius of 1.5 μm (see the top curve in Fig. 4). The basic shape of the reflectivity modulation does not depend on the radius of the micropillar; however, the smaller the radius, the higher the noise and the more pronounced the peak at τ_0 associated with the sample surface surrounding the micropillar. Finally, calculations show the first phononic stop band arising from the DBRs at 18 GHz [32] and so we conclude, that the observed modulation is not related to any mechanical resonance.

The comparison of the experimental results with the simulations show that our model is valid for probing interfaces in photonic structures with acoustic pulses. The response can be modeled solely by the interface displacement effect according to Eq. 4 for a relatively long acoustic pulse. Shortening the strain pulse obviously brings high-frequency phonons into play and the photoelastic effect should be taken into account, too. When the reflectivity modulation in the bulk GaAs aside from the micropillar is recorded, the 42 GHz Brillouin oscillation is clearly observed (see the inset in Fig. 4). However, no oscillations with frequencies corresponding to the GaAs/AlAs DBRs, which should be about 41 GHz, are observed when the micropillar is probed. This indicates that there are no high-frequency phonon components in the acoustic pulse propagating in the micropillar. A possible explanation might be a strong scattering of high frequency phonons at imperfections in the micropillar walls and its foot. The reflectivity modulation does not depend strongly on the shape and the duration of the modeled acoustic pulse. The simulations are independent of whether a Gaussian displacement profile or a shockwave acoustic pulse, whose high-frequency components have been filtered by the micropillar, are assumed (see the supplemental content).

The proposed method is applicable to manifold kinds of multilayered photonic device, where in depth information is of interest. If choosing a transparent probe wavelength, the maximum available depth is limited only by the penetration depth of the acoustic pulse. This length is governed by the acoustic mismatch at the internal interfaces, if the structure is cooled down and phonon attenuation becomes negligible. It is favorable to work with long acoustic pulses containing no high-frequency phonons, which lead to coherent Brillouin-oscillations. Unlike micropillars, most photonic devices do not suppress these phonons and a more sophisticated generation process is necessary. One might employ a pump wavelength with a longer absorption length, for example.

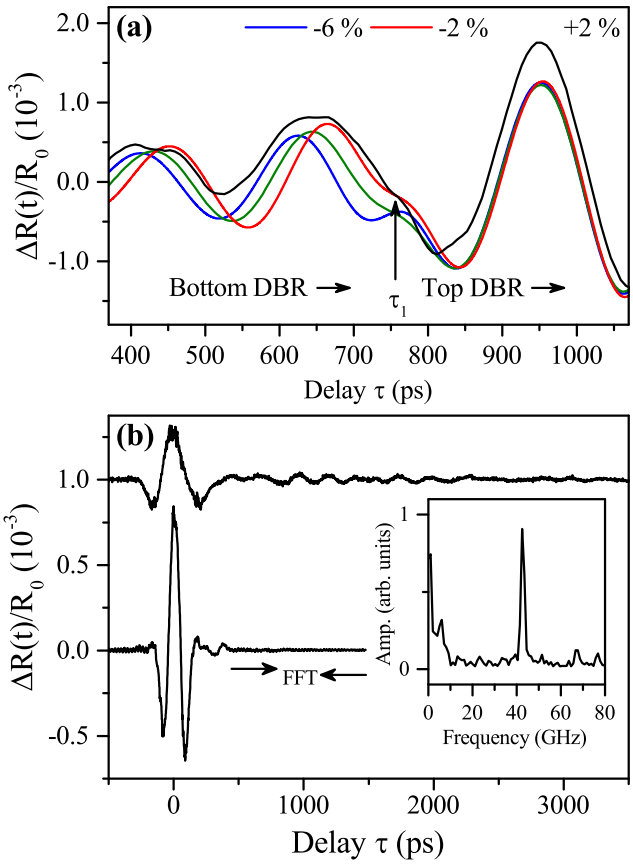

Fig. 4. Error and validity of the method. Panel (a): Simulations for the AlAs/GaAs micropillar for different cavity layer thicknesses. The experimental curve (black line) is vertically shifted for clarity. Panel (b): Experimental measurement of the reflectivity change in a thin AlAs/GaAs micropillar with a radius of 1.5 μm (top) and aside a micropillar (bottom). Next to the micropillar clear coherent Brillouin-oscillations are observed in the FFT (inset).

In conclusion, we presented a method for the characterization of a photonic device based on in-depth sensing the internal light field distribution with a picosecond acoustic pulse. We established experimental conditions under which we can treat the response of a given photonic mode to the acoustic pulse in a simplified and analytical way. From the recorded reflectivity modulation for the selected optical wavelength, we can deduce information on the internal light field distribution. In a last step, we reconstructed the original photonic device in a reverse-engineering procedure from the information we obtained about the light field. The technique was discussed in simulations for

a planar microcavity as an intuitive model structure and afterwards validated by experiments performed on an AlAs/GaAs micropillar resonator. From the simulation we were able to determine the layer thicknesses with a high precision of a few nm.

FUNDING INFORMATION

This work was supported by the Deutsche Forschungsgemeinschaft (TRR 142 Project A6 and TRR 160 Project B6) and the state of Bavaria. A.V.A. acknowledges the Alexander von Humboldt Foundation. M.B. acknowledges partial financial support from the Russian Ministry of Science and Education (contract No.14.Z50.31.0021).

REFERENCES

1. V. Huet, A. Rasoloniaina, P. Guillemé, P. Rochard, P. Féron, M. Mortier, A. Levenson, K. Bencheikh, A. Yacomotti, and Y. Dumeige, "Millisecond photon lifetime in a slow-light microcavity," Phys. Rev. Lett. **116**, 133902 (2016).
2. D. Press, S. Götzinger, S. Reitzenstein, C. Hofmann, A. Löffler, M. Kamp, A. Forchel, and Y. Yamamoto, "Photon antibunching from a single quantum-dot-microcavity system in the strong coupling regime," Phys. Rev. Lett. **98**, 117402 (2007).
3. R. Johne, N. A. Gippius, G. Pavlovic, D. D. Solnyshkov, I. A. Shelykh, and G. Malpuech, "Entangled photon pairs produced by a quantum dot strongly coupled to a microcavity," Phys. Rev. Lett. **100**, 240404 (2008).
4. S. Kim, B. Zhang, Z. Wang, J. Fischer, S. Brodbeck, M. Kamp, C. Schneider, S. Höfling, and H. Deng, "Coherent polariton laser," Phys. Rev. X **6**, 011026 (2016).
5. A. Kavokin, J. Baumberg, G. Malpuech, and F. Laussy, *Microcavities* (Oxford Science Publications, 2007), chap. 2.
6. P.-A. Mante, Y.-R. Huang, S.-C. Yang, T.-M. Liu, A. A. Maznev, J.-K. Sheu, and C.-K. Sun, "THz acoustic phonon spectroscopy and nanoscopy by using piezoelectric semiconductor heterostructures," Ultrasonics **56**, 52–65 (2015).
7. K.-H. Lin, C.-M. Lai, C.-C. Pan, J.-I. Chyi, J.-W. Shi, S.-Z. Sun, C.-F. Chang, and C.-K. Sun, "Spatial manipulation of nanoacoustic waves with nanoscale spot sizes," Nat. Nanotechnol. **2**, 704–708 (2007).
8. T. Dehoux, K. Ishikawa, P. H. Otsuka, M. Tomoda, O. Matsuda, M. Fujiwara, S. Takeuchi, I. A. Veres, V. E. Gusev, and O. B. Wright, "Optical tracking of picosecond coherent phonon pulse focusing inside a sub-micron object," Light Sci. Appl. **5**, e16082 (2016).
9. S. Danworaphong, M. Tomoda, Y. Matsumoto, O. Matsuda, T. Ohashi, H. Watanabe, M. Nagayama, K. Gohara, P. H. Otsuka, and O. B. Wright, "Three-dimensional imaging of biological cells with picosecond ultrasonics," Appl. Phys. Lett. **106**, 163701 (2015).
10. A. Fainstein, N. D. Lanzillotti-Kimura, B. Jusserand, and B. Perrin, "Strong optical-mechanical coupling in a vertical GaAs/AlAs microcavity for subterahertz phonons and near-infrared light," Phys. Rev. Lett. **110**, 037403 (2013).
11. A. Yamamoto, T. Mishina, Y. Masumoto, and M. Nakayama, "Coherent oscillation of zone-folded phonon modes in GaAs-AlAs superlattices," Phys. Rev. Lett. **73**, 740 (1994).
12. A. Bartels, T. Dekorsy, H. Kurz, and K. Köhler, "Coherent zone-folded longitudinal acoustic phonons in semiconductor superlattices: excitation and detection," Phys. Rev. Lett. **82**, 1044 (1999).
13. S. H. Lee, A. L. Cavalieri, D. M. Fritz, M. C. Swan, R. S. Hegde, M. Reason, R. S. Goldman, and D. A. Reis, "Generation and propagation of a picosecond acoustic pulse at a buried interface: time-resolved X-ray diffraction measurements," Phys. Rev. Lett. **95**, 246104 (2005).
14. O. Matsuda, T. Tachizaki, T. Fukui, J. J. Baumberg, and O. B. Wright, "Acoustic phonon generation and detection in GaAs/$Al_{0.3}Ga_{0.7}As$ quantum wells with picosecond laser pulses," Phys. Rev. B **71**, 115330 (2005).
15. H. J. Maris, "Picosecond Ultrasonics," Scientific American **278**, 86–89 (1998).
16. N. D. Lanzillotti-Kimura, A. Fainstein, B. Perrin, and B. Jusserand, "Theory of coherent generation and detection of THz acoustic phonons using optical microcavities," Phys. Rev. B **84**, 064307 (2011).
17. V. Villafane, P. Soubelet, A. E. Bruchhausen, N. D. Lanzillotti-Kimura, B. Jusserand, A. Lemaître, and A. Fainstein, "Slow light and slow acoustic phonons in optophononic resonators," Phys. Rev. B **94**, 205308 (2016).
18. O. Matsuda, M. C. Larciprete, R. L. Voti, and O. B. Wright, "Fundamentals of picosecond laser ultrasonics," Ultrasonics **56**, 3–20 (2015).
19. O. Matsuda, O. B. Wright, D. H. Hurley, V. Gusev, and K. Shimizu, "Coherent shear phonon generation and detection with picosecond laser acoustics," Phys. Rev. B **77**, 224110 (2008).
20. A. Bruchhausen, J. Lloyd-Hughes, M. Hettich, R. Gebs, M. Grossmann, O. Ristow, A. Bartels, M. Fischer, M. Beck, G. Scalari, J. Faist, A. Rudra, P. Gallo, E. Kapon, and T. Dekorsy, "Investigation of coherent acoustic phonons in terahertz quantum cascade laser structures using femtosecond pump-probe spectroscopy," J. Appl. Phys. **112**, 033517 (2012).
21. P. J. S. van Capel, E. Péronne, and J. I. Dijkhuis, "Nonlinear ultrafast acoustics at the nano scale," Ultrasonics **56**, 36–51 (2015).
22. C. Thomsen, H. T. Grahn, H. J. Maris, and J. Tauc, "Picosecond interferometric technique for study of phonons in the brillouin frequency range," Opt. Commun. **60**, 55–58 (1986).
23. P. Winter, A. Fainstein, B. Jusserand, B. Perrin, and A. Lemaître, "Optimized optical generation and detection of superlattice acoustic phonons," Appl. Phys. Lett. **94**, 103103 (2009).
24. K. Mizoguchi, T. Hino, M. Nakayama, T. Dekorsy, A. Bartels, H. Kurz, and S. Nakashima, "Umklapp process in observation of coherent folded longitudinal acoustic phonons in a GaAs/AlAs long-period superlattice," Physica E **21**, 646 (2004).
25. A. Devos and R. Côte, "Strong oscillations detected by picosecond ultrasonics in silicon: evidence for an electronic-structure effect," Phys. Rev. B **70**, 125208 (2004).
26. G. E. Jellison Jr., "Optical functions of GaAs, GaP, and Ge determined by two-channel polarization modulation ellipsometry," Opt. Mater. **1**, 151–160 (1992).
27. J. M. Gérard, B. Sermage, B. Gayral, B. Legrand, E. Costard, and V. Thierry-Mieg, "Enhanced spontaneous emission by quantum boxes in a monolithic optical microcavity," Phys. Rev. Lett. **81**, 1110 (1998).
28. C. Thomsen, J. Strait, Z. Vardeny, H. J. Maris, J. Tauc, and J. J. Hauser, "Coherent phonon generation and detection by picosecond light pulses," Phys. Rev. Lett. **53**, 989 (1984).
29. W. Chen, H. J. Maris, Z. R. Wasilewski, and S.-I. Tamura, "Attenuation and velocity of 56 GHz longitudinal phonons in gallium arsenide from 50 to 300 K," Philos. Mag. B **70**,

687–698 (1994).
30. L. D. Landau, L. P. Pitaevskii, A. M. Kosevich, and E. M. Lifshitz, *Theory of elasticity* (Butterworth-Heinemann, 1984).
31. M. Hu, X. Wang, G. V. Hartland, P. Mulvaney, J. P. Juste, and J. E. Sader, "Vibrational response of nanorods to ultrafast laser induced heating: theoretical and experimental analysis," J. Am. Chem. Soc. **125**, 14925 (2003).
32. S. Tamura, D. C. Hurley, and J. P. Wolfe, "Acoustic-phonon propagation in superlattices," Phys. Rev. B **38**, 1427 (1988).